Characterizing the Influence of Crystal Orientation on Surface Recombination in Silicon Wafers

Hang Cheong Sio, Teck Kong Chong, Sachin R. Surve, Klaus J. Weber, and Daniel H. Macdonald

***Abstract*—We present two approaches for evaluating the influence of crystal orientation on surface passivation of silicon wafers using photoluminescence imaging. The methods allow a variety of orientations that are not limited to (1 0 0) and (1 1 1) planes to be studied. The first approach is based on imaging carrier lifetimes in silicon strips containing different surface orientations that have been created from a single monocrystalline silicon wafer via laser cutting. The second approach is based on imaging carrier lifetimes among different grains in multicrystalline silicon wafers, which make use of their random distribution of crystal orientations. Both approaches are demonstrated with silicon-oxide-passivated samples. The results from both methods are consistent with each other, showing that the studied silicon oxide films provide a better passivation on surfaces with higher surface energy, such as (1 0 0) or (1 0 6) surfaces, compared with those with lower surface energy, such as (2 3 5) or (1 1 1) surfaces. The advantages and limitations of both approaches are also discussed and compared.**

***Index Terms*—Crystallography, dielectric films, photoluminescence, silicon, surfaces.**

I. Introduction

SURFACE passivation is important in solar cell manufacturing as it reduces surface recombination and, thus, improves the overall cell performance. Surface passivation is commonly achieved by depositing or growing dielectric films on silicon surfaces. Since the surfaces of an actual solar cell are usually textured to reduce its reflectance and enhance light trapping, surface passivation is typically applied to textured surfaces rather than planar surfaces. Such textured surfaces contain crystalline facets with orientations different from the untextured planar orientation. For example, random pyramid textured surfaces contain (1 1 1)-orientated facets as a result of the associated alkaline etching used. It has been reported that the passivation effectiveness for certain dielectric films, such as silicon dioxide [1], amorphous silicon [2], [3], and aluminum oxide [4], [5] can indeed be influenced by surface orientation, whereas some other films such as silicon nitride [1], [6] are unaffected. Baker-Finch and McIntosh [1] compared the passivation effectiveness on (1 0 0) and (1 1 1) wafers and observed the recombination rate at hydrogenated SiO_2-passivated planar (1 1 1) surfaces to be four times higher, compared with equivalent (1 0 0) surfaces, while a similar level of passivation was observed on planar (1 0 0) and planar (1 1 1) wafers passivated by silicon nitride, both before and after hydrogenation.

The majority of previous studies on dielectric passivation focused on monocrystalline silicon and were, therefore, usually limited to (1 0 0)-, (1 1 1)-, and (1 1 0)-orientated wafers. The effectiveness of surface passivation in multicrystalline silicon (mc-Si) material is more complex due to the random crystal orientation in mc-Si and the fact that commercial mc-Si solar cells are usually textured in an acidic, isotropic etchant, resulting in the formation of hemispherically shaped bowl-like structures on the surfaces [7], which contain a continuous range of crystal orientations. In this paper, we present two approaches to quantitatively evaluate the influence of surface orientation, not limited to only (1 0 0), (1 1 1), and (1 1 0) planes, on the passivation quality using photoluminescence (PL) imaging. PL imaging is a fast, nondestructive, and spatially resolved measurement technique, which allows accurate determination of the carrier lifetime [8]–[10], among many other applications [11].

The first approach is based on imaging carrier lifetimes in silicon strips containing different surface orientations, created from a single monocrystalline silicon wafer via laser cutting. The second approach is based on a previously demonstrated method for imaging surface recombination velocities (S_{eff}) among different grains in mc-Si wafers [12]. We revisit this method in this work and incorporate a recently proposed carrier desmearing technique [13], as explained in detail below, to eliminate unwanted measurement artefacts in the method and to significantly improve its accuracy. For demonstration, both approaches are applied to investigate the orientation-dependent passivation effect of thermal grown silicon oxide films. The advantages and limitations for both approaches are discussed and compared.

Manuscript received September 9, 2015; revised October 27, 2015 and November 30, 2015; accepted December 4, 2015. Date of publication December 21, 2015; date of current version February 18, 2016. This work was supported by the Australian Research Council (ARC) under Project RND009. The work of H. C. Sio was supported through a scholarship from BT Imaging and the Australian Renewable Energy Agency through the Australian Centre for Advanced Photovoltaics. The work of D. Macdonald was supported by an ARC Future Fellowship.

The authors are with the Research School of Engineering, College of Engineering and Computer Science, Australian National University, Canberra, A.C.T. 0200, Australia (e-mail: kelvin.sio@anu.edu.au; teck.chong@anu.edu.au; sachin.surve@anu.edu.au; klaus.weber@anu.edu.au; daniel.macdonald@anu.edu.au).

Color versions of one or more of the figures in this paper are available online at http://ieeexplore.ieee.org.

Digital Object Identifier 10.1109/JPHOTOV.2015.2508238

II. Method I: Imaging Carrier Lifetimes in Silicon Strips

A. Method Description

The principle of the first approach is demonstrated in Fig. 1. The starting material is a (1 1 0) p-type boron-doped Czochralski (Cz) grown monocrystalline silicon with a thickness of 1 mm. The background doping of the sample is around 3.6×10^{16} cm^{-3}. We cut the monocrystalline silicon wafer to produce multiple narrow strips in the wafer frame, as shown in Fig. 1, using a Coherent Scientific PRISMA 532-V Diode-Pumped Solid-State Laser, operating at 532 nm with nominal

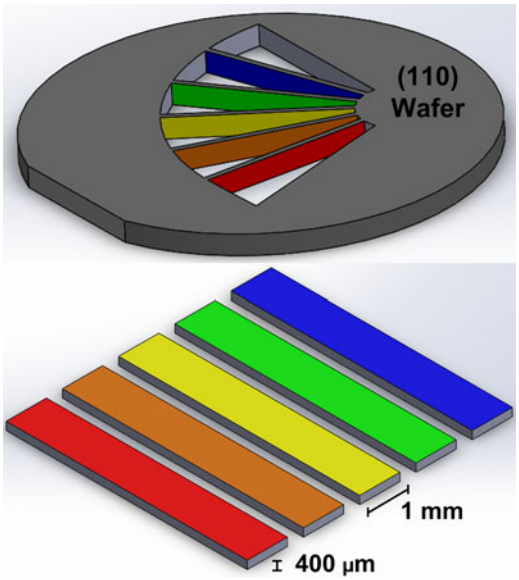

Fig. 1. Silicon strips created from a (1 1 0)-oriented monocrystalline silicon wafer through laser cutting. Note that the diagram is not to scale for visual illustration purposes.

pulsed power in the range of 12 W at 30 kHz. The width of the strips was approximately 400 μm. The cutting pattern was designed so that there is a slight rotation angle between each strip. This allows each silicon strip to have a different surface orientation of its sidewalls, denoted by different colors in Fig. 1. The orientation of the sidewall is determined by the laser cutting angle relative to the wafer flat, as well as the surface orientation of the wafer used, (1 1 0) in this case. Any orientation, in principle, can be achieved via perpendicular cut through a set of (1 0 0), (1 1 1), and (1 1 0) wafers.

After cutting, the entire wafer, with the strips still attached, was chemically etched for more than 5 min using HF and HNO_3 in a ratio of 1:10 to remove the surface damage from laser cutting. The width of the strips was reduced from 400 μm to around 307 μm after etching. After chemical cleaning, the wafer was then subjected to a thermal oxidation at 860 °C for 70 min, followed by a 3-h nitrogen anneal at the same temperature and a forming gas anneal at 400 °C for 30 min afterward, to grow silicon oxide films on its front, rear, and side surfaces. Instead of a more typical oxidation process, this lower oxidation temperature was used to avoid bulk degradation in the mc-Si wafers used in Method II, as described in detail below. The nitrogen and forming gas anneals afterward were used to improve the passivation quality of the silicon oxide films.

The thickness of the silicon oxide films was measured to be around 22 nm on the (1 1 0) surface, using an ellipsometer. Note that the oxidation rate varies on surfaces with different orientations and was found to decrease in order of $R_{(111)} > R_{(110)} > R_{(100)}$ [14]. We expect a variation in the oxide thickness from around 15 nm for the (1 0 0) surface to around 25 nm for the (1 1 1) surface. This range of variation in the oxide thickness is unlikely to impact the passivation quality, confirmed by the fact that the highest lifetime was in fact observed from the (1 0 0) surface, with the thinnest oxide, as shown below. In [1], it is also demonstrated that the passivation quality of silicon oxide is independent of oxide thickness after forming gas anneal. We chose to grow silicon oxide films of this thickness range to ensure the oxide is thick enough even on a (1 0 0) surface to achieve good passivation, but still thin enough that there is negligible variation in the reflectance among the different strips, which could impact the extracted lifetime values from PL images.

After oxidation, the strips were detached from the wafer frame, flipped by 90° and imaged with a PL imaging tool. The surface morphology of the strips was evaluated with an optical microscope, verifying that planar surfaces were achieved on all the strips with no observable difference among the different strips. A 1-mm-thick wafer was chosen for this work to maximize the width of the silicon strips after flipping and preventing the strips from becoming too narrow to be imaged, considering the spatial resolution of our PL imaging setup.

B. Characterization Method

The size of the silicon strips presents challenges in lifetime measurements. The silicon strips are too small, less than 900 μm wide after etching, to be measured with a typical Quasi-Steady-State Photoconductance (QSSPC) lifetime tester [15]. In this work, the effective lifetime of each strip was extracted from calibrated PL images. PL images in this work were captured using a BT Imaging LIS-R1 tool with a magnification lens, giving a lateral spatial resolution of 22 μm per pixel. An 808-nm laser was used for carrier excitation. The emitted PL was captured by a Silicon CCD camera. A short pass filter with a cutoff wavelength of 1050 nm was fitted in the imaging lens to reduce the impact of lateral light scattering both within the sample itself and within the camera's CCD chip. Image deconvolution using an experimentally determined point-spread function was applied to the PL images to further reduce the impact of image blurring caused by crosstalk in the CCD chip [16].

Since the strips are significantly smaller than the standard QSSPC sensor coil, it is not possible to perform QSSPC lifetime measurement on the silicon strips in order to acquire a calibration constant for the PL images. In this work, PL images were calibrated into absolute lifetime images based on an optically corrected calibration constant extracted from separate monocrystalline calibration wafers. The details of the calibration method are described in [17]. The surface orientations of the monocrystalline and multicrystalline samples were measured by electron back-scattered diffraction (EBSD), taken with a Zeiss UltraPlus analytical FESEM.

1) Extraction of the Surface Recombination Velocity (S_{eff}): For samples with uniform carrier density profile depthwise [18], the surface recombination velocity (S_{eff}) can be related to the bulk lifetime (τ_b) and the effective lifetime (τ_{eff}) according to

$$\frac{1}{\tau_{\text{eff}}(\Delta n)} = \frac{1}{\tau_b(\Delta n)} + \frac{2S_{\text{eff}}(\Delta n)}{W} \tag{1}$$

where W is the sample thickness.

The effective lifetime is the directly measurable parameter. The extraction of S_{eff} from the effective lifetime measurement

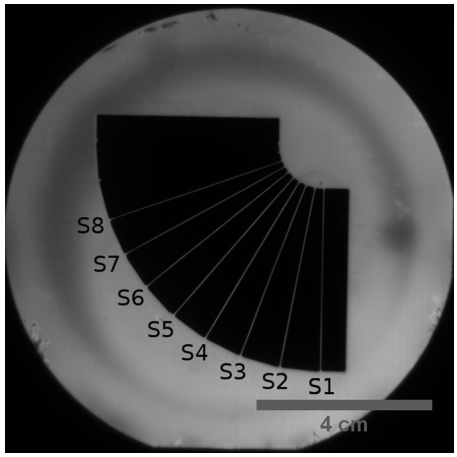

Fig. 2. PL image of silicon strips before being detached from the monocrystalline silicon wafer frame.

requires the bulk lifetime to be known. We used a (1 0 0) float-zone (FZ) wafer of similar resistivity, which received the same passivation as the silicon strips, as a control wafer to determine the bulk lifetime of the silicon strips. The $S_{\rm eff}$ of the FZ control wafer is calculated, as a function of excess carrier density, by subtracting the bulk lifetime, which is assumed to be Auger limited [19], from the measured injection-dependent effective lifetime according to (1). The Auger limit assumption in effect yields an upper bound for $S_{\rm eff}$. A silicon strip with a (1 0 0)-orientated surface is then assumed to have the same $S_{\rm eff}$ as the control wafer, and together with the effective lifetime measurement of that particular strip, the injection-dependent bulk lifetime of the silicon strips can be determined. By assuming that all the silicon strips have the same bulk lifetime, as they were cut from the same wafer, $S_{\rm eff}$ of each strip can be calculated.

C. Results

Fig. 2 shows a PL image of a monocrystalline silicon wafer that has been laser cut and thermally oxidized. Fig. 3(a) shows a PL-calibrated lifetime image of the silicon strips after being detached from the monocrystalline silicon wafer frame and flipped by 90°. Fig. 3(b) shows a line scan of the lifetimes across these silicon strips. A significant lifetime variation among different silicon strips can be observed. Note that the lifetime values in Fig. 3(b) were extracted at a constant generation rate; their injection levels can be different owing to their lifetime variation. The injection dependence of the lifetimes was determined from PL images captured at different laser intensities.

Table I shows the highest measured lifetime of each strip extracted at an excess carrier density of 1×10^{15} $\rm cm^{-3}$ and its corresponding $S_{\rm eff}$ value extracted using the method explained above. The lifetimes were measured from the center region in the strips far away from the edge so that the influence of surface recombination in the sidewall (a (1 1 0) surface in this case) is minimal. The highest lifetime values were chosen to avoid those darker regions of the strips, which show some bulk lifetime degradation. Note also that there is a slight variation ($\ll 5\%$) in

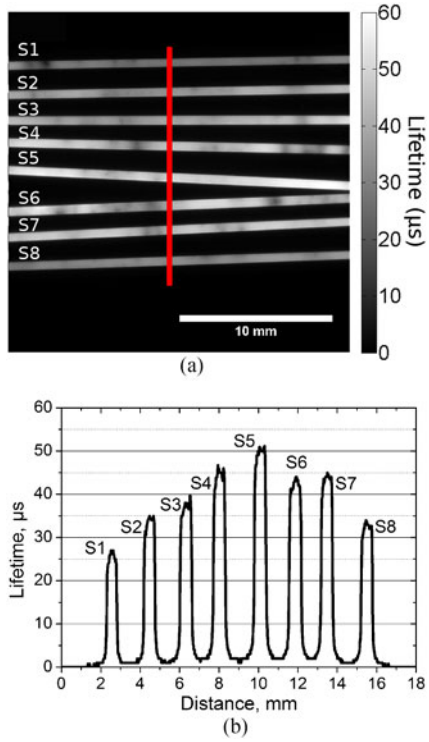

Fig. 3. (a) PL calibrated lifetime image of silicon strips after being detached from the wafer frame and flipped by 90°. The images were taken with incident photon flux of 2.7×10^{18} $\rm cm^{-2}{\cdot}s^{-1}$. (b) Line scan of the lifetimes across various silicon strips.

TABLE I
CRYSTAL ORIENTATION, SURFACE ENERGY, EFFECTIVE LIFETIME, AND SURFACE RECOMBINATION VELOCITY OF EACH SILICON STRIP

Strips	Orientation	Surface Energy (J/m^2)	$\tau_{\rm eff}$ at 1×10^{15} $\rm cm^{-3}$ (µs)	$S_{\rm eff}$ (cm/s)
S1	(2 3 5)	1.74	23	328
S2	(2 1 4)	1.90	29	187
S3	(1 0 3)	2.11	33	120
S4	(1 0 6)	2.18	34	106
S5	(1 0 0)	2.26	37	71
S6	(0 1 3)	2.11	34	106
S7	(2 1 5)	2.00	33	121
S8	(1 1 2)	1.78	27	214

Details on the calculation of the surface energy can be found in [20]. A bulk lifetime of 44 μs (determined using a control sample with the method stated above) was used in the calculation of the $S_{\rm eff}$ values.

the thickness among different strips. The average thickness of 307 μm was used in the calculation of the $S_{\rm eff}$ values.

Also shown is the crystal orientation, measured with EBSD, of each silicon strip and its corresponding surface energy. Details on the calculation of the surface energy can be found in our previous work in [20]. From Table I, it can be seen that the passivation quality of the studied silicon oxide films is strongly influenced by the crystal orientation. Among the eight studied orientations, the $S_{\rm eff}$ value of the (1 0 0)-orientated strip is the lowest. The $S_{\rm eff}$ values vary from 71 cm/s for the (1 0 0) surface to 328 cm/s for the (2 3 5) surface.

It should be noted that during the calculation of the $S_{\rm eff}$ values with (1), it is assumed that the carrier density profile is

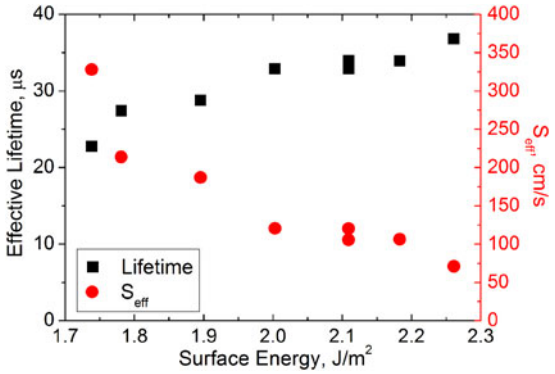

Fig. 4. Effective lifetime and surface recombination velocity of each studied silicon strip classified according to its corresponding surface energy.

uniform depthwise. This is not strictly true for the Cz samples used in this work, owing to the relatively low bulk lifetime of the wafer. However, this only leads to an uncertainty of less than 5% (determined using numerical simulations with details presented in [21], based on a bulk lifetime of 44 μs and the measured effective lifetimes) in the extracted S_{eff} values. Such uncertainty can be further reduced by using wafers with higher lifetime. The boron–oxygen-related defect is likely to be the cause for the low lifetime in the studied Cz wafer, given that the measured lifetimes correlate well with literature-reported lifetimes after defect activation [22], which is likely to have occurred to the studied Cz samples during the repeated PL measurements.

Fig. 4 correlates the effective lifetimes and surface recombination velocities (S_{eff}) of the silicon strips with their corresponding surface energies. The surface energy gives an indication of the surface structure such as the density of dangling bonds. A clear trend can be observed between τ_{eff}, S_{eff}, and surface energy. The results here show that the studied silicon oxide films are more effective in passivating surfaces with high surface energy such as (1 0 0) or (1 0 6) surfaces and less effective in passivating surfaces with low surface energy such as a (2 3 5) surface. This is in agreement with previous studies [1], which observed that the passivation effectiveness of silicon oxide on a (1 0 0) surface is considerably higher than a (1 1 1) surface, which has a much lower surface energy [23]–[25]. The observed behavior could be related to the defect density at the interface. Arnold *et al.* [26] observed a dependence of surface state density on crystal orientation on thermally oxidized single crystal silicon.

III. Method II: Imaging Carrier Lifetimes in Multicrystalline Silicon Wafers

A. Method Description

In the second approach, we used different grains in mc-Si wafers as sources of different crystal orientations. N-type phosphorus-doped mc-Si wafers were used in this work. N-type mc-Si wafers were chosen due to their high bulk lifetime compared with p-type mc-Si wafers, which increases the sensitivity of the method. The high bulk lifetime also ensures that a uniform carrier density profile along the depth of the sample is achieved during lifetime measurements, satisfying (1). The mc-Si wafers have a background doping of around 1.2×10^{16} cm^{-3}.

After initial chemical etching to remove saw damage, the wafers were phosphorus gettered and hydrogenated to further improve their bulk lifetime. Phosphorus gettering was performed by subjecting the wafers to a 30-min $POCl_3$ diffusion at 880 °C, followed by an extended annealing in an N_2 ambient for more than 12 h at 600 °C in the same diffusion furnace. Hydrogenation was achieved by coating the samples with plasma-enhanced chemical vapor deposition silicon nitride films and firing them in a rapid thermal processing furnace (Unitemp UTP-1100) for 3 min at 700 °C in N_2 ambient. After gettering and hydrogenation, the surface films and diffused layers were removed via HF dip and chemical etching. Before oxidation, the samples were mirror polished through chemical etching using HF and HNO_3 in a ratio of 1:8. This was necessary since any variations in surface topology from grain to grain may have an impact on the passivation, as well as the reflectance and PL emission properties. Finally, the samples were subjected to a thermal oxidation, using the same recipe described above, to grow silicon oxide films on their surfaces and imaged with the PL system. The measurement setup is the same as that used in Method I. The thickness of the mc-Si wafers was reduced from 180 μm in the as-cut state to around 130 μm after processing.

B. Characterization Method

1) Carrier Smearing: Method II relies on imaging carrier lifetimes in various grains within a mc-Si wafer. Lateral diffusion of carriers within the sample causes a smearing effect in the acquired lifetime images, resulting in a significant underestimation of the extracted lifetime values for smaller grains and regions near GBs and other defects. While the lateral carrier diffusion is a real effect that occurs during normal solar cell operation, such smearing effects reduce the accuracy and resolution in studies on the recombination lifetimes, which is the objective of this work. In this work, we applied a recently proposed carrier desmearing technique [13] to the PL-calibrated lifetime images to correct for the influence of lateral carrier smearing within the sample and thus to allow more accurate extraction of the intragrain lifetime.

For demonstration, Fig. 5 shows a set of lifetime images of a silicon-oxide-passivated mc-Si wafer studied in this work before and after applying the carrier desmearing technique. Comparing the images, it can be seen that the lifetime image after desmearing is much sharper, especially around crystal defects and intergrain regions where there are large variations in the lifetime values. After desmearing, some smaller subgrains are observable and the lifetimes in the intragrain regions are also more uniform.

We are not able to apply the desmearing technique to the silicon strips used in Method I as the strips are too narrow, which significantly affects the accuracy of the noise filtering method used in the desmearing technique. In principle, the carrier smearing effect could lead to an underestimation of the extracted lifetime values from the silicon strips. However, such uncertainty is small given that the sidewalls of the silicon strips

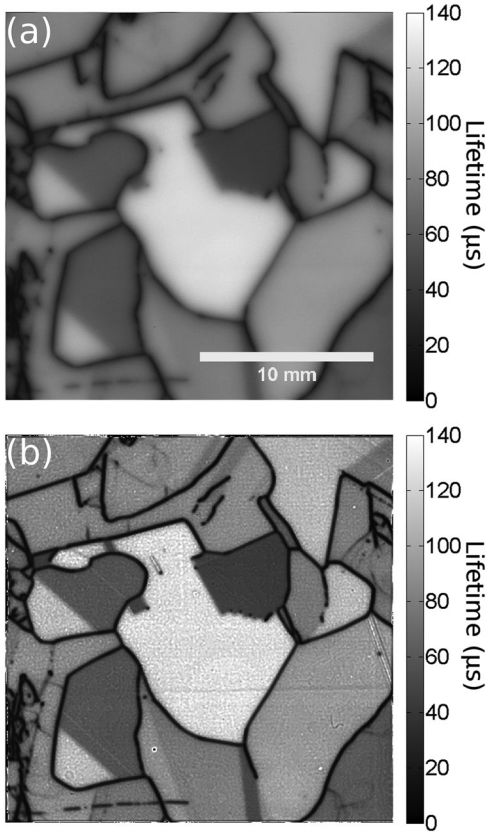

Fig. 5. PL calibrated lifetime images (a) before and (b) after applying the carrier desmearing technique. The images were taken with an incident photon flux of 2.7×10^{18} cm^{-2}·s^{-1}.

are also passivated with silicon oxide, unlike the grain boundaries in a mc-Si wafer, coupled with the fact that the Cz wafer used in Method I has a lower bulk lifetime than the mc-Si wafers used in Method II, resulting in a reduced impact of the carrier smearing effect.

2) Extraction of the Surface Recombination Velocity (S_{eff}): We applied a similar approach to Method I to extract the surface recombination velocities in the mc-Si samples from the measured lifetimes. A (1 0 0) grain in the mc-Si wafer was used together with an FZ control sample to estimate its bulk lifetime. By assuming that the bulk lifetime is uniform among the entire mc-Si wafer, S_{eff} of each grain can then be calculated using (1). Note that in contrast with Method I, where it is quite safe to assume that all silicon strips have the same bulk lifetime as they were cut from the same monocrystalline wafer, the bulk lifetime among different grains in a mc-Si wafer may indeed be different. This could contribute to uncertainty in the extracted S_{eff} values. This uncertainty is expected to be small as long as the rate of surface recombination is much higher than bulk recombination. In this work, such a surface-limited condition is achieved by using gettered and hydrogenated n-type mc-Si wafers with high intragrain bulk lifetime (above 700 μs measured after passivating with silicon nitride), combined with the fact that the studied silicon oxide films only provide moderate passivation. However, this could be a potential issue when applying the method to study dielectric films that provide very good passivation effect ($S_{\text{eff}} \ll 10$ cm/s), such as aluminum oxide, silicon nitride, or other silicon oxides, in which the varying impact of the bulk lifetime is comparable with that of S_{eff} among various grains. In such cases, method I is likely to be more accurate.

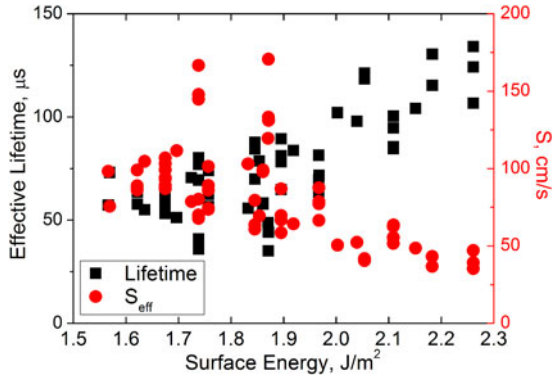

Fig. 6. Effective lifetimes and surface recombination velocities of individual grains in the studied mc-Si wafers classified according to their corresponding surface energies.

Note that the sensitivity limit of method II depends on the bulk lifetime and the thickness of the mc-Si wafers used. When applied on 130-μm-thick wafers with bulk lifetime varying from 500 μs to 1 ms between grains, an error of up to 16% is estimated in the extracted S_{eff} for a dielectric film with S_{eff} of 40 cm/s. Using thinner mc-Si wafers with higher bulk lifetime can further enhance the sensitivity of the method. For example, using 120-μm-thick wafers with bulk lifetime varying from 1 to 2 ms between grains can limit the error in the extracted S_{eff} to 15% or below for films with S_{eff} of 20 cm/s or higher.

C. Results

Fig. 5(b) shows a PL calibrated lifetime image of a silicon-oxide-passivated mc-Si wafer studied in this work. A strong contrast can be observed among different grains. We previously observed a similar contrast on mirror polished nonpassivated mc-Si wafers, in which we attributed to the orientation-dependent passivation effect of a very thin native oxide formed on their surfaces [20].

Fig. 6 compares the surface energies of selected gains (modeled based on their crystal orientations measured with EBSD) and their corresponding lifetimes and S_{eff}. It can be seen that there is a strong correlation between the surface energy of each grain and its corresponding S_{eff} value, suggesting that the contrasts observed in Fig. 5(b) are indeed due to the orientation dependence of the passivation. Similar to the results obtained from Method I, orientations with a higher surface energy show a lower S_{eff} value, and *vice versa*, although in this case, the scatter in the data is significantly larger, possibly due to factors such as thickness variation across the mc-Si wafer as a result of the extended acidic etching used, uncertainty in the modeling of the surface energies or some impact of bulk lifetime variations from grain to grain.

Owing to the simplicity of this method, a large number of grains/orientations can be studied with this approach. A total of 66 grains were analyzed in this work. Based on these

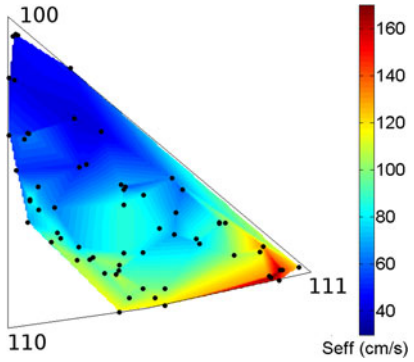

Fig. 7. Interpolated result of the surface recombination velocity of each orientation plotted in an IPF based on measured grains, represented by dark dots.

66 grains, we interpolated the surface recombination velocities of various crystal orientations in an inverse pole figure (IPF) for the studied silicon oxide films. The results are shown in Fig. 7. It can be observed that the passivation quality of the studied silicon oxide is best for surfaces close to (1 0 0) orientation, and its effectiveness reduces gradually as the orientation moves toward the (1 1 1) plane. Note that we did not detect any grains at or close to (1 1 0) orientation among the analyzed grains.

IV. Discussion

Both of the presented methods show that the passivation effectiveness of the studied silicon oxide films is strongly crystal orientation dependent. In general, the surface recombination rate depends on the doping level/type of the substrate, the charge in the dielectric film, and their interaction. Owing to the variation in the background doping level and type of the samples used, we could not directly compare the S_{eff} values extracted from both methods. Nevertheless, the results from both methods are qualitatively consistent with each other. The lower S_{eff} values on the mc-Si samples could be related the positive charge in the oxide layer [27], which allows a better passivation on n-type samples owing to field-effect passivation, or due to the different doping concentrations or types in the substrates [28], interacting with the electron and hole capture cross sections at the interface.

Comparing both approaches, the advantage of Method I is that there is negligible variation in the bulk lifetimes among different strips as they were cut from the same monocrystalline wafer. However, it requires a more complex sample preparation procedure. The sample size is also limited. On the other hand, Method II is simple and easy to implement, thus allowing a large number of orientations to be studied. However, as mentioned above, it relies on the assumption that any varying impact of the bulk lifetime is significantly less than the variation of surface recombination among the mc-Si grains. While this assumption is largely valid for the silicon-oxide-passivated samples studied in this work, it may not be when applying the method to other dielectric films with lower surface recombination velocities.

V. Conclusion

We have presented two methods for evaluating the orientation dependent passivation effect of dielectric films. The impact of various crystal orientations, which are not limited only to (1 0 0) and (1 1 1) planes, can be studied through the proposed methods. The first method is based on imaging carrier lifetimes in silicon strips cut from a single monocrystalline silicon wafer. The second method is based on imaging carrier lifetimes among different grains in mc-Si wafers. Both methods were applied on thermally grown silicon oxide films. The results from both methods agree qualitatively with each other, showing that the studied silicon oxide films provide a better passivation on surfaces with higher surface energy, such as (1 0 0) surface, compared to those with lower surface energy, such as (1 1 1) surface. The presented methods could be applied on other dielectric films such as silicon nitride or aluminum oxide to investigate their corresponding orientation-dependent passivation effect.

Acknowledgment

H. C. Sio would like to thank T. C. Kho and S. P. Phang for assistance with sample preparation.

References

[1] S. C. Baker-Finch and K. R. McIntosh, "The contribution of planes, vertices, and edges to recombination at pyramidally textured surfaces," *IEEE J. Photovoltaics*, vol. 1, no. 1, pp. 59–65, Jul. 2011.

[2] U. K. Das, M. Z. Burrows, M. Lu, S. Bowden, and R. W. Birkmire, "Surface passivation and heterojunction cells on Si (100) and (111) wafers using DC and RF plasma deposited Si:H thin films," *Appl. Phys. Lett.*, vol. 92, art. no. 063504, 2008.

[3] A. Descoeudres *et al.*, "Improved amorphous/crystalline silicon interface passivation by hydrogen plasma treatment," *Appl. Phys. Lett.*, vol. 99, art. no. 123506, 2011.

[4] W. Liang *et al.*, "Surface passivation of boron-diffused P-type silicon surfaces with (1 0 0) and (1 1 1) orientations by ALD Al_2O_3 layers," *IEEE J. Photovoltaics*, vol. 3, no. 2, pp. 678–683, Apr. 2013.

[5] L. E. Black, T. C. Kho, K. R. McIntosh, and A. Cuevas, "The influence of orientation and morphology on the passivation of crystalline silicon surfaces by Al2O3," *Energy Procedia*, vol. 55, pp. 750–756, 2014.

[6] W. Yimao and K. R. McIntosh, "On the surface passivation of textured C-Si by PECVD silicon nitride," *IEEE J. Photovoltaics*, vol. 3, no. 4, pp. 1229–1235, Oct. 2013.

[7] D. H. Macdonald *et al.*, "Texturing industrial multicrystalline silicon solar cells," *Sol. Energy*, vol. 76, pp. 277–283, 2004.

[8] T. Trupke, R. A. Bardos, M. C. Schubert, and W. Warta, "Photoluminescence imaging of silicon wafers," *Appl. Phys. Lett.*, vol. 89, art. no. 044107, 2006.

[9] S. Herlufsen, J. Schmidt, D. Hinken, K. Bothe, and R. Brendel, "Photoconductance-calibrated photoluminescence lifetime imaging of crystalline silicon," *Phys. Status Solidi (RRL)—Rapid Res. Lett.*, vol. 2, pp. 245–247, 2008.

[10] J. A. Giesecke, M. C. Schubert, B. Michl, F. Schindler, and W. Warta, "Minority carrier lifetime imaging of silicon wafers calibrated by quasi-steady-state photoluminescence," *Sol. Energy Mater. Sol. Cells*, vol. 95, pp. 1011–1018, 2011.

[11] T. Trupke *et al.*, "Progress with luminescence imaging for the characterisation of silicon wafers and solar cells," presented at the 22nd Eur. Photovoltaic Sol. Energy Conf., Milan, Italy, 2007.

[12] H. C. Sio *et al.*, "The influence of crystal orientation on surface passivation in multi-crystalline silicon," in *Proc. 39th IEEE Photovoltaic Spec. Conf.*, Tampa, FL, USA, 2013, pp. 1770–1775.

[13] S. P. Phang, H. C. Sio, and D. Macdonald, "Carrier de-smearing of photoluminescence images on silicon wafers using the continuity equation," *Appl. Phys. Lett.*, vol. 103, art. no. 192112, 2013.

[14] E. A. Irene, H. Z. Massoud, and E. Tierney, "Silicon oxidation studies: Silicon orientation effects on thermal oxidation," *J. Electrochem. Soc.*, vol. 133, pp. 1253–1256, 1986.

[15] R. A. Sinton and A. Cuevas, "Contactless determination of current–voltage characteristics and minority-carrier lifetimes in semiconductors from quasi-steady-state photoconductance data," *Appl. Phys. Lett.*, vol. 69, pp. 2510–2512, 1996.

[16] D. Walter *et al.*, "The impact of silicon CCD photon spread on quantitative analyses of luminescence images," *IEEE J. Photovoltaics*, vol. 4, no. 1, pp. 368–373, Jan. 2014.
[17] H. C. Sio, S. P. Phang, T. Trupke, and D. Macdonald, "An accurate method for calibrating photoluminescence-based lifetime images on multi-crystalline silicon wafers," *Sol. Energy Mater. Sol. Cells*, vol. 131, pp. 77–84, 2014.
[18] A. G. Aberle, *Crystalline Silicon Solar Cells: Advanced Surface Passivation Analysis*. Sydney, Australia: Centre Photovoltaic Eng., Univ. New South Wales, 1999.
[19] A. Richter, S. W. Glunz, F. Werner, J. Schmidt, and A. Cuevas, "Improved quantitative description of Auger recombination in crystalline silicon," *Phys. Rev. B*, vol. 86, art. no. 165202, Oct. 9, 2012.
[20] H. C. Sio, Z. Xiong, T. Trupke, and D. Macdonald, "Imaging crystal orientations in multicrystalline silicon wafers via photoluminescence," *Appl. Phys. Lett.*, vol. 101, art. no. 082102, 2012.
[21] H. C. Sio, T. Trupke, and D. Macdonald, "Quantifying carrier recombination at grain boundaries in multicrystalline silicon wafers through photoluminescence imaging," *J. Appl. Phys.*, vol. 116, art. no. 244905, 2014.
[22] K. Bothe, R. Sinton, and J. Schmidt, "Fundamental boron–oxygen-related carrier lifetime limit in mono- and multicrystalline silicon," *Prog. Photovoltaics, Res. Appl.*, vol. 13, pp. 287–296, 2005.
[23] R. J. Jaccodine, "Surface energy of germanium and silicon," *J. Electrochem. Soc.*, vol. 110, pp. 524–527, 1963.
[24] G. H. Lu, M. Huang, M. Cuma, and F. Liu, "Relative stability of Si surfaces: A first-principles study," *Surface Sci.*, vol. 588, pp. 61–70, 2005.
[25] A. A. Stekolnikov, J. Furthmüller, and F. Bechstedt, "Absolute surface energies of group-IV semiconductors: Dependence on orientation and reconstruction," *Phys. Rev. B*, vol. 65, art. no. 115318, 2002.
[26] E. Arnold, J. Ladell, and G. Abowitz, "Crystallographic symmetry of surface state density in thermally oxidized silicon," *Appl. Phys. Lett.*, vol. 13, pp. 413–416, 1968.
[27] A. G. Aberle, S. Glunz, and W. Warta, "Impact of illumination level and oxide parameters on Shockley–Read–Hall recombination at the Si-SiO2 interface," *J. Appl. Phys.*, vol. 71, pp. 4422–4431, 1992.
[28] S. W. Glunz, A. B. Sproul, W. Warta, and W. Wettling, "Injection-level-dependent recombination velocities at the Si-SiO_2 interface for various dopant concentrations," *J. Appl. Phys.*, vol. 75, pp. 1611–1615, 1994.

Authors' photographs and biographies not available at the time of publication.